Shi *et al.*
Chinese Journal of Mechanical Engineering (2024) 37:26
https://doi.org/10.1186/s10033-024-01008-6

Chinese Journal of Mechanical Engineering

ORIGINAL ARTICLE

Open Access

Model Parameters Identification and Backstepping Control of Lower Limb Exoskeleton Based on Enhanced Whale Algorithm

Yan Shi[1], Jiange Kou[1*], Zhenlei Chen[2], Yixuan Wang[1] and Qing Guo[2*]

Abstract

Exoskeletons generally require accurate dynamic models to design the model-based controller conveniently under the human-robot interaction condition. However, due to unknown model parameters such as the mass, moment of inertia and mechanical size, the dynamic model of exoskeletons is difficult to construct. Hence, an enhanced whale optimization algorithm (EWOA) is proposed to identify the exoskeleton model parameters. Meanwhile, the periodic excitation trajectories are designed by finite Fourier series to input the desired position demand of exoskeletons with mechanical physical constraints. Then a backstepping controller based on the identified model is adopted to improve the human-robot wearable comfortable performance under cooperative motion. Finally, the proposed Model parameters identification and control are verified by a two-DOF exoskeletons platform. The knee joint motion achieves a steady-state response after 0.5 s. Meanwhile, the position error of hip joint response is less than 0.03 rad after 0.9 s. In addition, the steady-state human-robot interaction torque of the two joints is constrained within 15 N · m. This research proposes a whale optimization algorithm to optimize the excitation trajectory and identify model parameters. Furthermore, an enhanced mutation strategy is adopted to avoid whale evolution's unsatisfactory local optimal value.

Keywords Parameter identification, Enhanced whale optimization algorithm (EWOA), Backstepping, Human-robot interaction, Lower limb exoskeleton

1 Introduction

The key aspects of the current exoskeleton research are focused on quality, security, and stability. Reliable exoskeleton control and cooperative motion realization require an accurate dynamic model [1, 2]. Meanwhile, the advanced controllers such as position, speed and torque loop also depend on model accuracy to improve the cooperative motion performance. The wearable comfortable performance is determined by the time-varying torque of human-robot interaction, which should be real-time constrained in a tiny range by the designed controller [3, 4]. In addition, many robot manufacturers do not provide these model parameters or only obtain partial parametric information [5]. Due to the irregular bionic structure, the exoskeleton's physical parameters such as centroids, moments of inertia and mechanical size are difficult to measure in practice. Hence, parameter identification is an effective approach to obtaining an accurate exoskeleton model before the controller design.

*Correspondence:
Jiange Kou
koujiange@buaa.edu.cn
Qing Guo
guoqinguestc@uestc.edu.cn
[1] School of Automation Science and Electrical Engineering, Beihang University, Beijing 100191, China
[2] School of Aeronautics and Astronautics, University of Electronic Science and Technology of China, Chengdu 611731, China

It is well recognized that the model identification method is commonly used in mechanical motion plants. There are several approaches to estimating the dynamic parameters. For instance, the maximum likelihood estimation methods [6, 7] and least squares estimation methods are popular methods to obtain the high-accuracy original model [8, 9]. The statistical parameter is fit by these two methods, but not to be suitable for very complex models, such as exoskeleton dynamic models. Some other methods include the extended Kalman filter [10] and Bayesian neural networks [11, 12] are also used in robot and grey-box thermal models. Furthermore, many other estimation methods are also proposed to address model uncertainty and external load based on least squares, such as the total least squares [13], weighted least squares [10, 14] and the online recursive estimation method [15]. In these methods, joint angle and torque can be directly measured, but joint velocity and acceleration must be pre-estimated. The designed observer and estimators [16], especially the zero-phase bandpass filter [17, 18] are commonly used to improve the output performance.

The design of excitation trajectory is necessary for general robot identification [19] due to plant physical constraints. The excitation trajectory is provided to sufficiently estimate the accurate model parameters under unknown disturbances [20]. Han et al. [21] proposed an iterative approach with the weighted least squares (WLS). This method iteratively used the least squares to address the nonlinear friction model constrained by linear matrix inequality (LMI). Hence, the measurement noise can be properly rejected in controller design. Lee et al. [22] presented a parameter identification method to generate a random excitation trajectory of a robot manipulator joint based on recursive least squares (RLS). Gao [23] used an iterative identification process based on the least square method and obtained more than 80% reduction of motion uncertainty. Most of these methods are designed for industrial robots and acquire appropriate identification parameters. However, the exoskeleton cannot be accurately modeled due to a strong human-robot coupling system with a fast cooperative motion response [24, 25].

In this study, a 2-DOF lower limb exoskeleton was constructed to realize the human-robot cooperative motion. This 2-DOF rehabilitation exoskeleton is primarily geared towards patients with subacute or early-stage problems. Although some problems with muscle contraction and coordination have been observed, this group of patients still has the ability to move. It can be used to complete cooperative human-machine rehabilitation training. Inspired by previous studies about the identification and control method, the exoskeleton's active control mode is studied to improve the wearable comfortable performance between the operator and exoskeleton. The main contributions of this paper are twofold.

(1) The periodic excitation trajectories are designed by a finite Fourier series to consider the mechanical physical constraint of human-robot cooperative motion. A whale optimization algorithm is presented to optimize the excitation trajectory and identify model parameters. Furthermore, an enhanced mutation strategy is adopted to avoid whale evolution's unsatisfactory local optimal value. To the authors' best knowledge, the enhanced whale optimization algorithm (EWOA) is a new method to identify the exoskeleton model parameters.
(2) The backstepping controller is designed to realize the active control mode of the exoskeleton based on the identified dynamic model to improve the wearable comfortable performance of the operator. The dynamic and steady-state response is guaranteed by the proposed control scheme in a two-DOF exoskeletons platform.

The remainder of this paper is organized as follows. The exoskeleton dynamics and its transformed model are constructed in Section 2. The excitation trajectory design and the EWOA algorithm are described in Section 3. Then the parameter identification, the backstepping controller and experimental verification are introduced in Section 4. Finally, the conclusions are drawn in Section 5.

2 Identification Model Framework

2.1 Model Identification and Control Scheme

This study presents an identification method using an enhanced whale algorithm to identify the model parameters of the exoskeleton. Then a backstepping controller is designed based on the identification model as shown in Figure 1.

Firstly, the Lagrange model of exoskeleton is constructed to separate unknown parameters and the measured information, such as joint torque and angle obtained by some sensors. Subsequently, a finite Fourier series is used to design the periodic excitation trajectory based on the physical constraints of the exoskeleton. Then the EWOA is applied to optimize the parameters of the excitation trajectory. In the presence of unknown model parameters, PID control is initially employed in excitation experiments to acquire Input/Output (I/O) datasets. Using these datasets, the EWOA is employed to identify the model parameters. Finally, based on the identified dynamic model, a backstepping controller is designed to manipulate the exoskeleton to follow a random demand

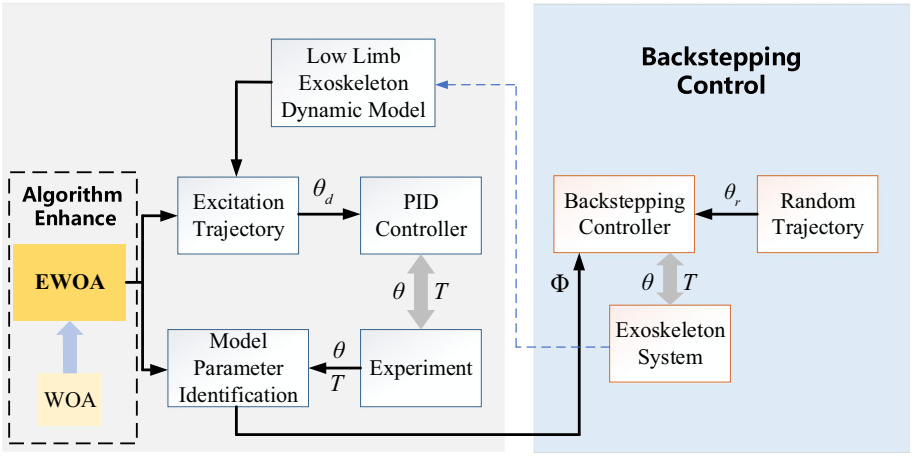

Figure 1 Model identification and backstepping control scheme

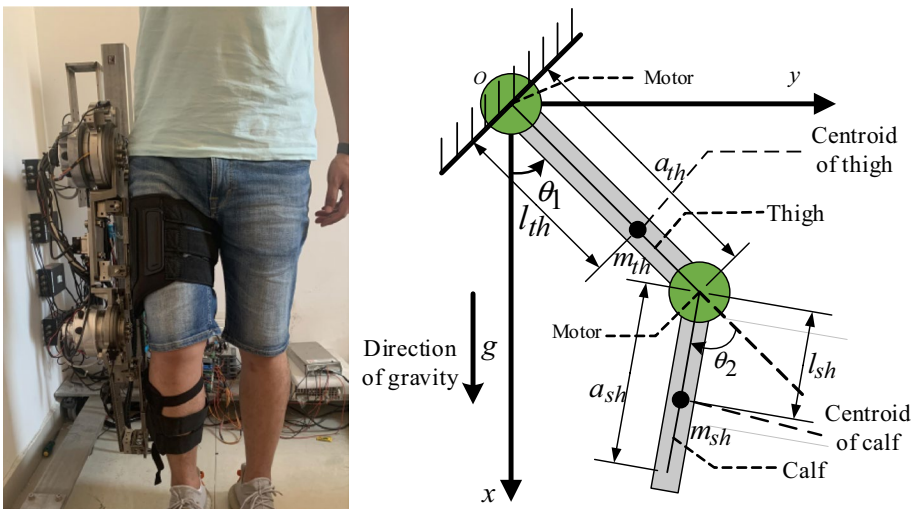

Figure 2 The theoretical and physical model of the lower limb exoskeleton system

trajectory with satisfactory wearable comfortable performance.

2.2 Lagrange Modeling

This theoretical and physical model of the lower limb exoskeleton is shown in Figure 2. The exoskeleton is a typical second-order state feedback system, which is mainly composed of controllers, sensors, actuators, and various auxiliary devices. The centroid positions of thigh and calf in Cartesian coordinate system are expressed by (X_1, Y_1), (X_2, Y_2), and the related variables are shown in Table 1.

According to the geometric relationship, the relationship between joint coordinates and its centroid is given by

Table 1 Parameters and definitions in exoskeleton

Parameter	Definition	Unit
θ_1	Rotation angle of hip joint	rad
θ_2	Rotation angle of knee joint	rad
a_{th}	Length of thigh	m
a_{sh}	Length of calf	m
m_{th}	Quality of thigh	kg
m_{sh}	Quality of calf	kg
l_{th}	Distance from hip joint to thigh centroid	m
l_{sh}	Distance from knee joint to calf centroid	m
I_{m1}	Inertia of the thigh	kg/m^2
I_{m2}	Inertia of the calf	kg/m^2
g	Acceleration of gravity	m/s^2
$\theta = [\theta_1, \theta_2]$	Position information of exoskeleton joints	–

$$\begin{cases} X_1 = l_{th}\cos(\theta_1), \\ Y_1 = l_{th}\sin(\theta_1), \\ X_2 = a_{th}\cos(\theta_1) + l_{sh}\cos(\theta_1+\theta_2), \\ Y_2 = a_{th}\sin(\theta_1) + l_{sh}\sin(\theta_1+\theta_2). \end{cases} \tag{1}$$

The Lagrange equation of exoskeleton yields that

$$\begin{cases} L = K - P, \\ \tau = \dfrac{\partial}{\partial t}\dfrac{\partial L}{\partial \dot{\theta}} - \dfrac{\partial L}{\partial \theta}, \end{cases} \tag{2}$$

where L represents the total energy of Lagrangian system, K represents the system's kinetic energy, P represents the potential energy, and τ represents the external torque of the joint.

The driven torque of exoskeleton is described as

$$\boldsymbol{\tau} = [\tau_{hip}, \tau_{knee}]^{\mathrm{T}}, \tag{3}$$

where τ_{hip}, τ_{knee} represent the toque of hip and knee, respectively.

The dynamic equation of the two-DOF lower limb exoskeleton is constructed as

$$\boldsymbol{H}(\theta)\ddot{\theta} + \boldsymbol{C}(\theta,\dot{\theta})\dot{\theta} + \boldsymbol{G}(\theta) = \boldsymbol{\tau}, \tag{4}$$

where $\boldsymbol{H}(\theta)\ddot{\theta}, \boldsymbol{C}(\theta,\dot{\theta}), \boldsymbol{G}(\theta)$ are inertial matrix, Coriolis matrix, gravity matrix, respectively. They can be expressed as

$$\begin{cases} \boldsymbol{H} = \begin{bmatrix} H_{11} & H_{12} \\ H_{21} & H_{21} \end{bmatrix}, \\ \boldsymbol{C} = \begin{bmatrix} C_{11} & C_{12} \\ C_{21} & C_{22} \end{bmatrix}, \\ \boldsymbol{G} = \begin{bmatrix} G_1 \\ G_2 \end{bmatrix}. \end{cases} \tag{5}$$

In addition, the friction force exists in the exoskeleton dynamic model, which mainly considers the Coulomb friction and viscous friction items as

$$\boldsymbol{f}(\dot{\theta}) = \begin{bmatrix} k_{11}\mathrm{sgn}(\dot{\theta}_1) + k_{12}\dot{\theta}_1 \\ k_{21}\mathrm{sgn}(\dot{\theta}_2) + k_{22}\dot{\theta}_2 \end{bmatrix}, \tag{6}$$

where k_{11}, k_{21} represent the coulomb friction coefficients of the exoskeleton thigh and calf, respectively; k_{12}, k_{22} represent the viscous friction coefficient; sgn is the symbolic function.

Therefore, the whole exoskeleton model can be expressed as

$$\boldsymbol{H}(\theta)\ddot{\theta} + \boldsymbol{C}(\theta,\dot{\theta})\dot{\theta} + \boldsymbol{G}(\theta) + \boldsymbol{f}(\dot{\theta}) = \boldsymbol{\tau}. \tag{7}$$

2.3 Transformed Lagrangian Model

There exists an unknown parameter matrix $\boldsymbol{\Phi} \in \mathbb{R}^m$ involving mass, inertia, and mechanical size of exoskeleton. Here a linear relationship is firstly constructed between unknown parameters and the measured information, such as joint torque and angle obtained by some sensors, which is described as

$$\boldsymbol{H}(\theta)\dot{\xi} + \boldsymbol{C}(\theta,\dot{\theta})\boldsymbol{\xi} + \boldsymbol{G}(\theta) + \boldsymbol{f}(\dot{\theta}) = \boldsymbol{Y}(\theta,\dot{\theta},\boldsymbol{\xi},\dot{\xi})\boldsymbol{\Phi}, \tag{8}$$

where $\boldsymbol{Y}(\theta,\dot{\theta},\boldsymbol{\xi},\dot{\xi})$ is a regression matrix, and $\boldsymbol{\xi} \in \mathbb{R}^n$ is a differentiable vector.

For the exoskeleton robot, the state matrix $\boldsymbol{Y}$ and the parametric vector $\boldsymbol{\Phi}$ are expressed as

$$\boldsymbol{\Phi} = \left[\Phi^1, \Phi^2, \Phi^3, \Phi^4, \Phi^5, \Phi^6, \Phi^7, \Phi^8\right], \tag{9}$$

$$\boldsymbol{Y} = \begin{bmatrix} Y^{11}, Y^{12}, Y^{13}, Y^{14}, Y^{15}, Y^{16}, Y^{17}, Y^{18} \\ Y^{21}, Y^{22}, Y^{23}, Y^{24}, Y^{25}, Y^{26}, Y^{27}, Y^{28} \end{bmatrix}, \tag{10}$$

where

$$\begin{cases} \Phi^1 = I_{th} + I_{sh} + m_{th}l_{th}^2 + m_{sh}a_{th}^2 + m_{sh}l_{sh}^2, \\ \Phi^2 = I_{sh} + m_{sh}l_{sh}^2, \\ \Phi^3 = m_{sh}a_{th}l_{sh}, \\ \Phi^4 = m_{th}a_{th}l_{th} - I_{th} - m_{th}l_{th}^2, \end{cases} \tag{11}$$

and $\Phi^5 = k_{11}, \Phi^6 = k_{12}, \Phi^7 = k_{21}, \Phi^8 = k_{22}$, the state matrix $\boldsymbol{Y}$ is expressed as $Y^{11} = \ddot{\theta}_1 + e\sin\theta_1$, $Y^{12} = \ddot{\theta}_2 + e\sin\theta_1, Y^{13} = 2\cos\theta_2\ddot{\theta}_1 + \cos\theta_2\ddot{\theta}_2 - 2\sin\theta_2\dot{\theta}_1\dot{\theta}_2 - \sin\theta_2\dot{\theta}_2^2 + e\sin(\theta_1+\theta_2)$, $Y^{14} = e\sin\theta_1$, $Y^{15} = \mathrm{sgn}(\dot{\theta}_1)$, $Y^{16} = \dot{\theta}_1$, $Y^{22} = \ddot{\theta}_1 + \ddot{\theta}_2$, $Y^{23} = \cos\theta_2\ddot{\theta}_1 + \sin\theta_2\dot{\theta}_1^2 + e\sin(\theta_1+\theta_2)$, $Y^{27} = \mathrm{sgn}(\dot{\theta}_2)$, $Y^{28} = \dot{\theta}_2$, and $Y^{17}, Y^{18}, Y^{21}, Y^{24}, Y^{25}, Y^{26}$ is 0 in $\boldsymbol{Y}$, $e = g/a_{th}$ is the intermediate variable.

Hence, the model functions $\boldsymbol{H}$, $\boldsymbol{C}$, $\boldsymbol{G}$ are expressed as

$$\begin{cases} \boldsymbol{H} = \begin{bmatrix} \Phi^1 + 2\Phi^3\cos\theta_2 & \Phi^2 + \Phi^3\cos\theta_2 \\ \Phi^2 + \Phi^3\cos\theta_2 & \Phi^{(2)} \end{bmatrix}, \\ \boldsymbol{C} = \begin{bmatrix} -2\Phi^3\dot{\theta}_2\sin\theta_2 & -\Phi^3\dot{\theta}_2\sin\theta_2 \\ \Phi^3\dot{\theta}_1\sin\theta_2 & 0 \end{bmatrix}, \\ \boldsymbol{G} = \begin{bmatrix} \Phi^3 e\sin(\theta_1+\theta_2) + (\Phi^1 - \Phi^2 + \Phi^4)e\sin\theta_1 \\ \Phi^3 e\sin(\theta_1+\theta_2) \end{bmatrix}. \end{cases} \tag{12}$$

According to Eqs. (7) and (8), the transformed Lagrangian model of exoskeleton is given by

$$\boldsymbol{\tau} = \boldsymbol{Y}(\theta,\dot{\theta},\boldsymbol{\xi},\dot{\xi})\boldsymbol{\Phi}, \tag{13}$$

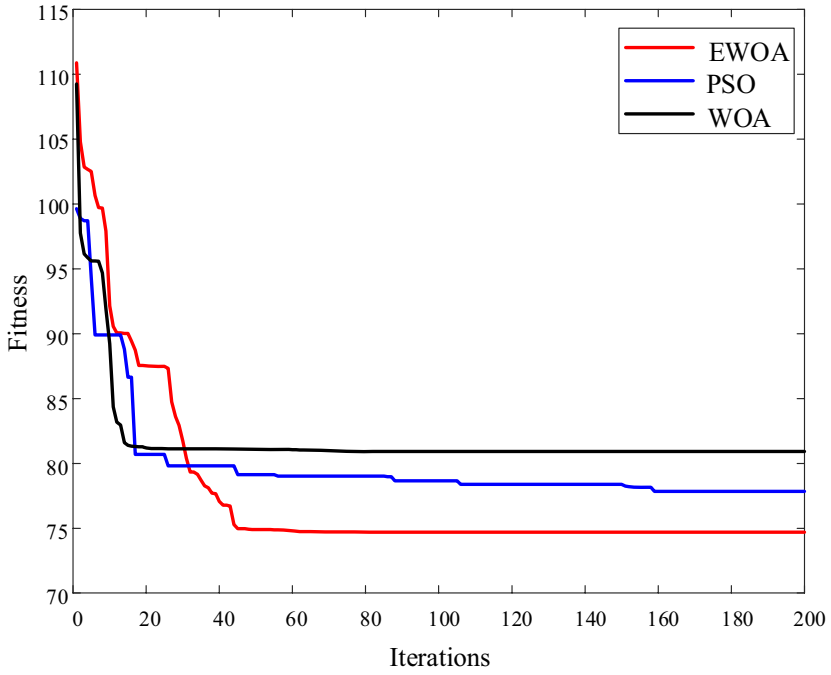

(a) The parameters optimization of excitation trajectory

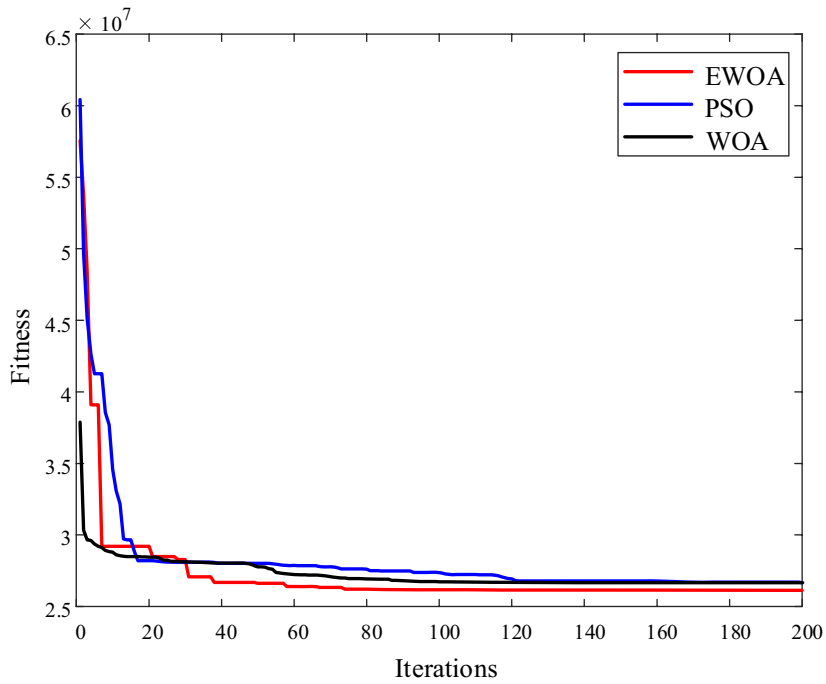

(b) Optimization of dynamic model parameters

Figure 3 The comparison results of different optimization algorithms

Table 2 The boundary conditions of exoskeleton

	Angle (rad)	Velocity (rad)	Acceleration (rad/s^2)
Thigh	[– 0.087, 1.309]	[– 1.645, 1.645]	[– 5.168, 5.168]
Calf	[– 1.658, –0.087]	[– 1.645, 1.645]	[– 5.168, 5.168]

where $\boldsymbol{\Phi}$ is the unknown parameters to be identified based on the regressive vector $\boldsymbol{\tau}$ and the state matrix $\boldsymbol{Y}$, which are obtained by sampling datasets.

3 EWOA Optimization and Excitation Trajectories Design

3.1 EWOA Optimization

The unknown parameters of the exoskeleton are separated from the measured state in Section 2. In the literature, there are several optimistic algorithms to identify system parameters, such as Particle Swarm Optimization (PSO) [26] and Whale Optimization Algorithm (WOA) [27]. This study proposes the Enhanced Whale Optimization Algorithm (EWOA) to identify model parameters. The algorithm feature simulates the optimization processing of the mathematical modeling related to humpback whale hunting [28].

In the whale algorithm, the position of each whale represents a feasible solution. Each whale has two behaviors during the hunting process: One is to surround the prey, which means all the whales move toward the prey. The other behavior is to create a bubble net, where the whales swim in a circle and eject bubbles to drive the prey away. Whales will randomly choose these two behaviors to hunt in each generation of swimming.

The position of each whale in the M-dimensional solution space is given by

$$X = (x_1, x_2, x_3, \cdots, x_M). \tag{14}$$

As the whale swims towards the optimal position in the process of surrounding prey, the position can be calculated as

$$X_i^{t+1} = X_{best}^t - \boldsymbol{A}\left|C * X_{best} - X_i^t\right|, \tag{15}$$

where X_{best} is the current optimal whale position; the dimension of $\boldsymbol{A}$ is a random number uniformly, which is distributed in $(-a, a)$. The initial value of a is 2, and it linearly decreases into 0 in the finite iterations number, C is a random number uniformly distributed in (0, 2).

After a group of whales swim towards the position of a random whale, the next iterative position is obtained as

$$X_i^{t+1} = X_{rand}^t - \boldsymbol{A}\left|C * X_{rand} - X_i^t\right|. \tag{16}$$

Table 3 The parameters of excitation trajectory

Parameter	Value	Parameter	Value
a_1	1.685	b_1	5.689
a_2	– 2.258	b_2	2.904
a_3	13.828	b_3	14.805
a_4	– 15.389	b_4	10.822
A_1	3.530	B_1	5.205
A_2	– 9.949	B_2	4.578
A_3	– 15.978	B_3	15.914
A_4	5.415	B_4	11.738

The swimming mode depends on the value of $\boldsymbol{A}$. In the other word, the whale chooses to swim toward the optimal individual as $|\boldsymbol{A}<1|$. Otherwise, it swims towards a random individual. During the hunting process, the bubble net is used to update the whale's position as

$$X_i^{t+1} = \left|X_{best}^t - X_i^t\right| * e^l * \cos(2\pi l) + X_{best}^t, \tag{17}$$

where l is a random number uniformly distributed in [– 1,1].

The local optimization problem quickly appears in the whale algorithm compared with the PSO algorithm, as shown in Figure 3(a). To avoid the local optimal solution, differential mutation was used to improve the total optimization performance. It is to be noted that the better individual whales are selected in the current population for mutation. This mutation way is described as Eq. (18), which can effectively expand the algorithm search domain and prevent the local optimal solution.

$$V_i(t+1) = X_i(t) + \phi(\boldsymbol{X}_{r1}(t) - \boldsymbol{X}_{r2}(t)), \tag{18}$$

where V represents the position of the ith whale; ϕ is a scaling factor; $\boldsymbol{X}_{r1}(t) - \boldsymbol{X}_{r2}(t)$ represents the difference vector of the whale position under the current iterations. The new mutated individual will be replaced the original individual as the better one.

In this study, WOA, PSO, and EWOA are all used to optimize the parameters, respectively. The population size of the algorithm is set to 100, and the maximum number of iterations is 200 as shown in Figure 3(a). The horizontal coordinate is the iteration number. The vertical coordinate represents the fitness value, i.e. the condition number of the state matrix $\boldsymbol{Y}$. The vertical coordinate is a small value means the better results of the excitation trajectory. Meanwhile, the three algorithms are used to optimize the unknown parameters ϕ of the exoskeleton dynamics model as shown in Figure 3(b).

The WOA converges fastest but easily falls into local optimal solution among three algorithms. Meanwhile, the convergence speed of the PSO algorithm in the initial stage

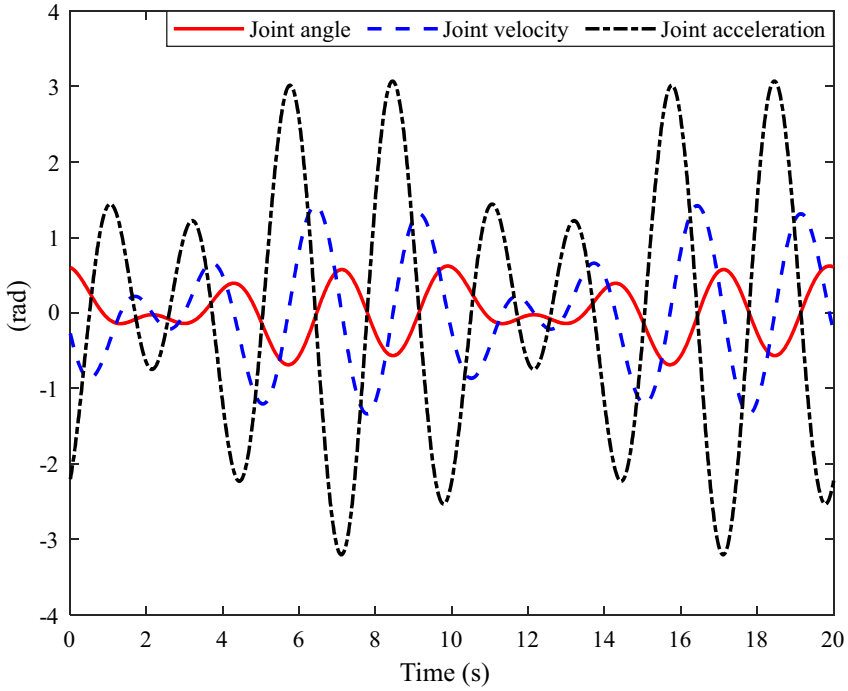

(a) Exoskeleton hip joint excitation trajectory optimized

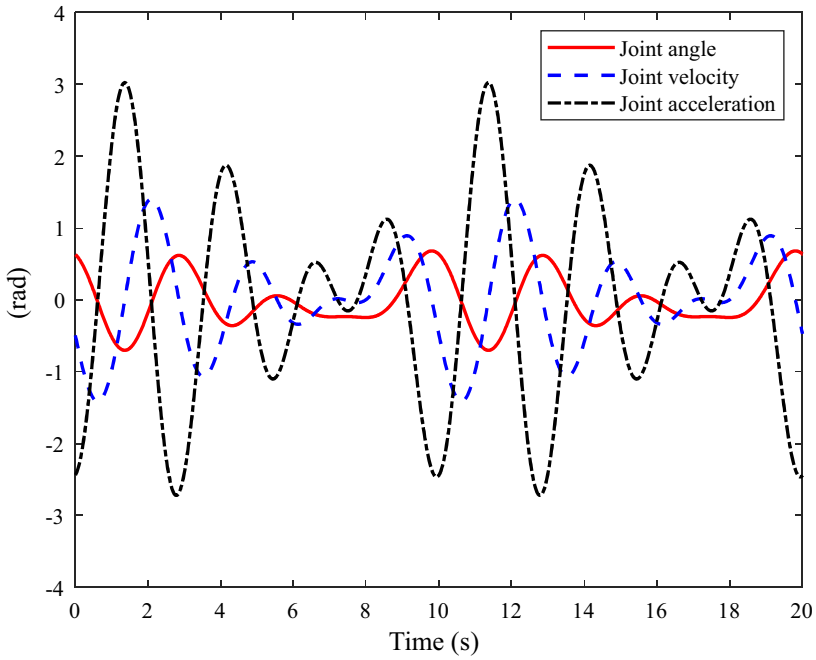

(b) Exoskeleton knee joint excitation trajectory optimized

Figure 4 Excitation trajectory optimized by EWOA

Table 4 Parameters of exoskeleton dynamic model

Parameter ($\widehat{\Phi}$)	Value
$\widehat{\Phi}_1$ (kg · m^2)	28.634
$\widehat{\Phi}_2$ (kg · m^2)	9.716
$\widehat{\Phi}_3$ (kg · m^2)	1.84
$\widehat{\Phi}_4$ (kg · m^2)	− 11.54
$\widehat{\Phi}_5$ (kg · m)	17.224
$\widehat{\Phi}_6$ (N · kg · s · rad^{-1})	− 3.1
$\widehat{\Phi}_7$ (kg · m)	33.372
$\widehat{\Phi}_8$ (N · kg · s · rad^{-1})	27.657

is faster than that of EWOA. However, the optimization solution of PSO is convergence with the increasing iterations. The convergence rate of the EWOA is slightly slower than the WOA, but the local optimal solution is obviously improved after 50 iterations.

3.2 Generation of Excitation Trajectories

The off-line identification has certain requirements for the experimental signal, which should fully excite all motion modes of the identified plant [20]. A reasonable excitation trajectory should consider the mechanical physical constraint. In the regression matrix $\boldsymbol{Y}(\theta, \dot{\theta}, \xi, \dot{\xi})$, external disturbance will emerge as a great influence on the identification results. Based on the Fourier series, the excitation trajectory is composed of finite sums of N harmonic sine and cosine functions, which is expressed as

$$\begin{cases} \theta_d = \theta_d + \sum_{\kappa=1}^{N} (a_\kappa \sin(\kappa\omega_f t) + b_\kappa \cos(\kappa\omega_f t)), \\ \dot{\theta}_d = \sum_{\kappa=1}^{N} \kappa\omega_f (a_\kappa \cos(\kappa\omega_f t) - b_\kappa \sin(\kappa\omega_f t)), \\ \ddot{\theta}_d = \sum_{\kappa=1}^{N} (\kappa\omega_f)^2 (-a_\kappa \sin(\kappa\omega_f t) - b_\kappa \cos(\kappa\omega_f t)), \end{cases} \tag{19}$$

where θ_d is the initial value of the joint, the initial value in the thigh θ_1 is 0.6107 rad, and the initial value in the calf θ_2 is -0.8727 rad ; θ_d, $\dot{\theta}_d$, $\ddot{\theta}_d$ represent the desired joint angle, angular velocity, angular acceleration, respectively; a_κ, b_κ are the coefficient of the Fourier series to be optimized, ω_f is the fundamental frequency, $N = 4$ is the Fourier series period.

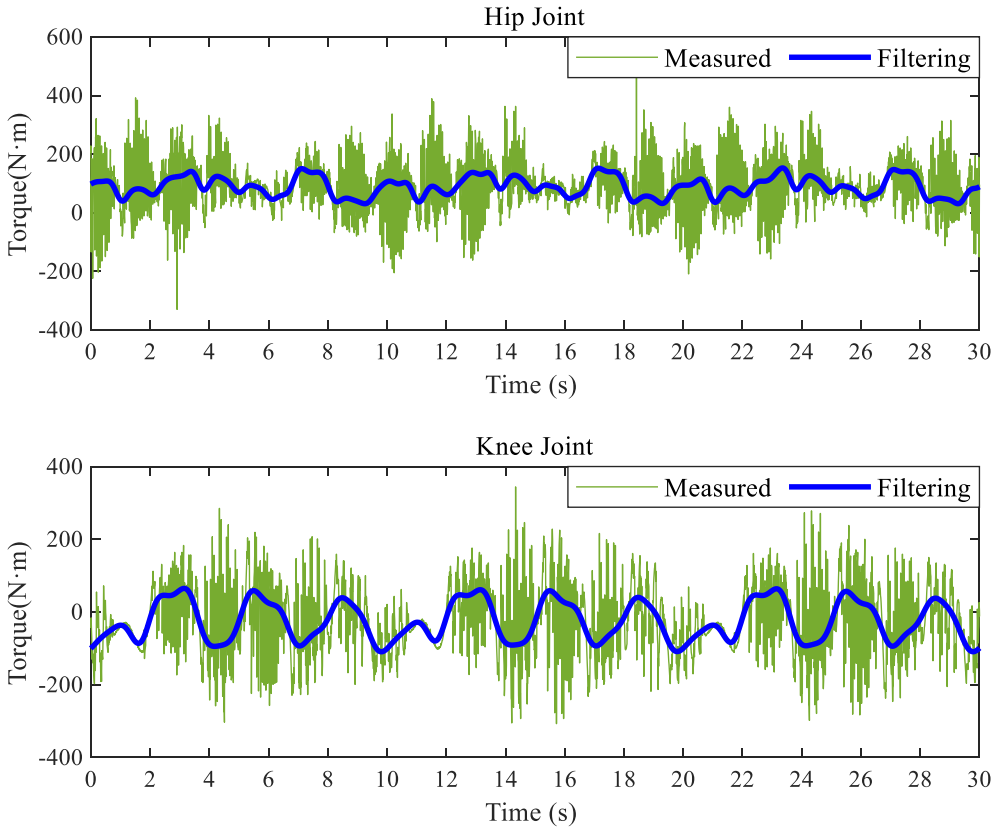

Figure 5 The measured joint torque based on Butterworth low-pass filter

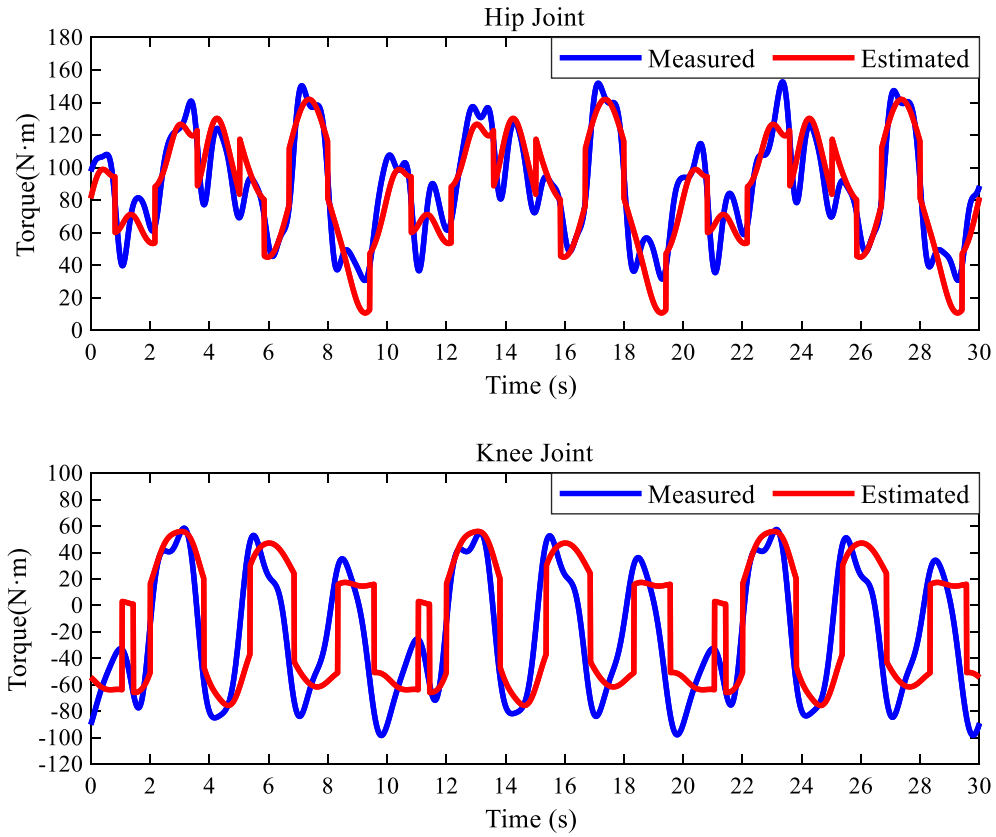

Figure 6 The estimated joint torque and the corresponding filtered signal

In addition, the exoskeleton needs to ensure the wearer's safety during the human-robot cooperative motion. The motion range must be limited during the exoskeleton's movement. Hence, the boundary conditions of the exoskeleton are shown in Table 2.

The objective of parametric identification is to obtain an optimization solution for the EWOA. An optimal criterion is used to find the periodic excitation trajectories based on the minimum condition number of the regression matrix [19, 29, 30]. Therefore, the condition number of the regression matrix is adopted as a fitness function in the algorithm optimization.

It can be expressed as

$$Fitness = K(Y) = \|Y\| \cdot \left\|Y^{-1}\right\|. \tag{20}$$

Based on a typical human gait, $\omega_f = 0.2\pi$ is substituted into the designed excitation trajectory Eq. (19). There are 16 parameters to be optimized. The minimum condition number of the regression matrix is selected as the final result of the EWOA. The final optimization solution of a_k, b_k (hip joint) and A_k, B_k (knee joint) are shown in Table 3.

The excitation trajectories of the exoskeleton two joints are obtained based on the optimized parameters shown in Figure 4. The angle position, velocity, and acceleration of the identified excitation trajectory are constrained in Table 2.

3.3 Model Parameter Identification

The excitation trajectory is selected as the desired trajectory demand of the exoskeleton. Furthermore, the PID controller drives the two-DOF lower limb exoskeleton experimental platform, as shown in Figure 2. The exoskeleton's joint position and real-time torque are obtained by the absolute encoders and torque sensors (integrating into the motor). Moreover, the obtained information is constructed as the dataset to identify the model parameters based on EWOA.

According to Eq. (13), and the current estimated parameter $\widehat{\boldsymbol{\Phi}}$ by EWOA, the estimated torque $\widehat{\boldsymbol{\tau}}$ is expressed as

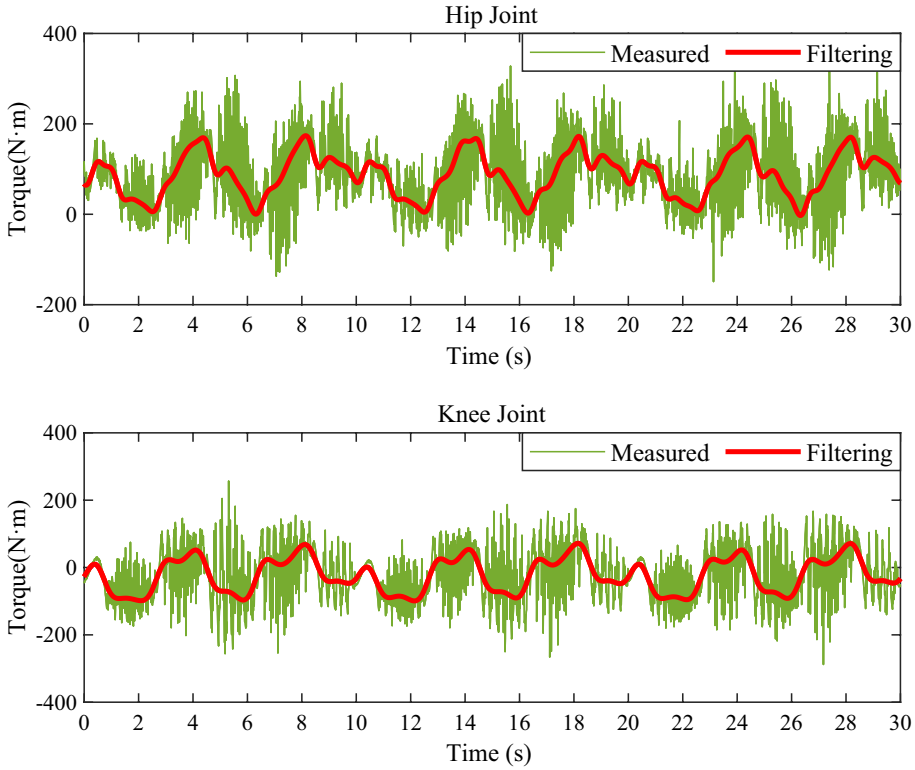

Figure 7 The measured joint torque and the corresponding filtered signal

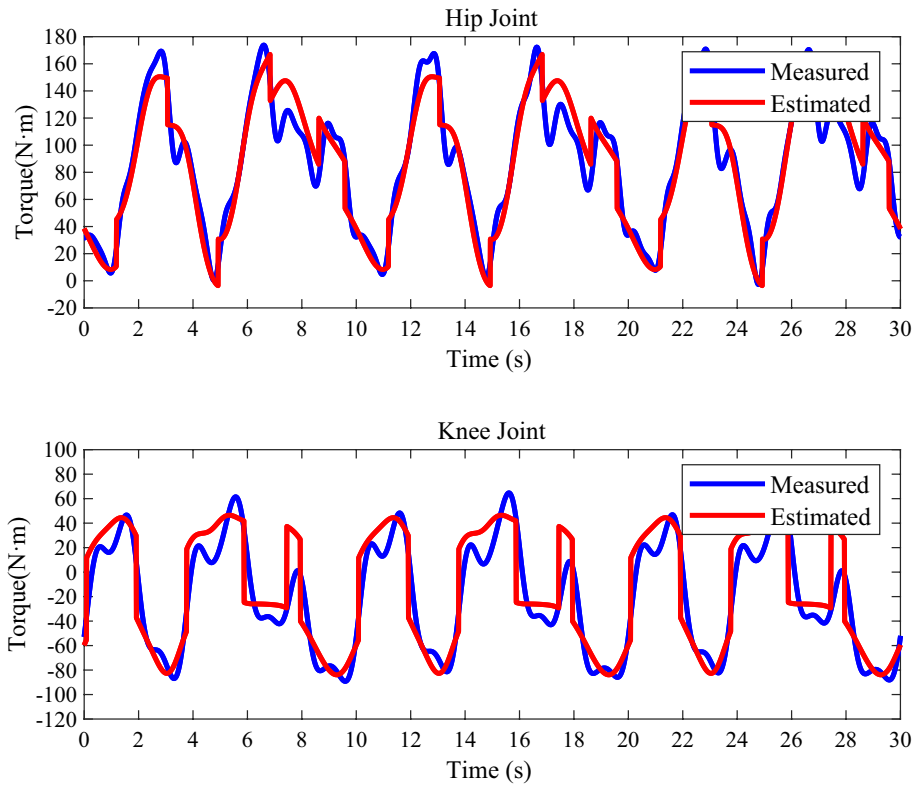

Figure 8 The comparison of measured and estimated joint torque

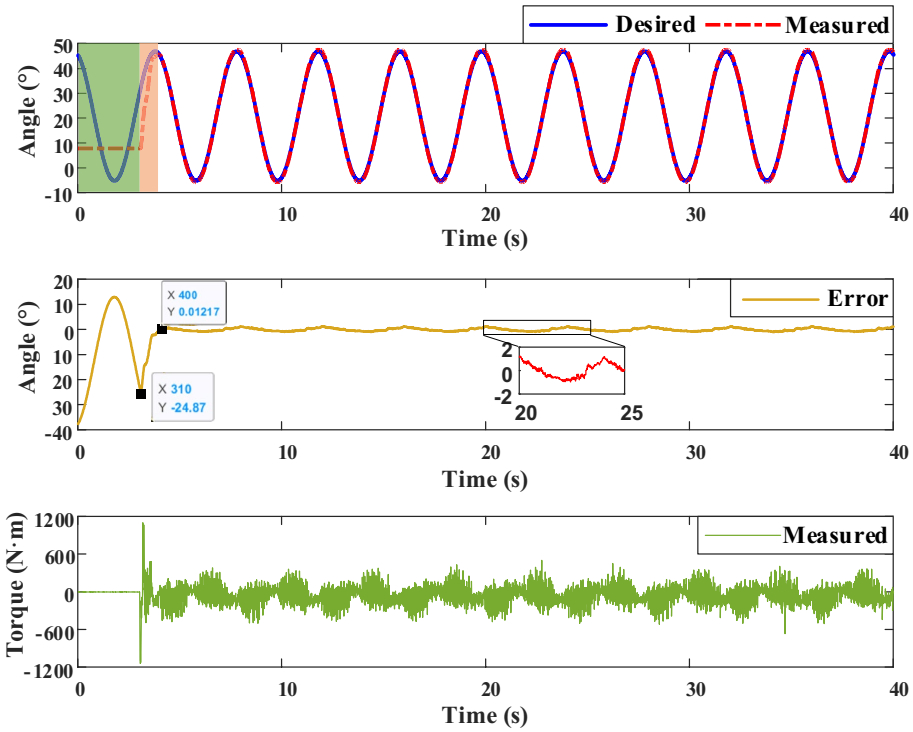

Figure 9 The joint position, and the corresponding position error, together with the measured torque of hip joint by using backstepping controller

$$\hat{\boldsymbol{\tau}} = \overline{\boldsymbol{Y}}\hat{\boldsymbol{\Phi}}, \tag{21}$$

where $\overline{\boldsymbol{Y}}$ is the element in the dataset. The error $\tilde{\tau} = \overline{\tau} - \hat{\tau}$ is the important basis for evaluating $\widehat{\boldsymbol{\Phi}}$. Therefore, the mean square deviations of calculated torque $\hat{\boldsymbol{\tau}}$ and measured torque $\overline{\boldsymbol{\tau}}$ are designed as a fitness function and $\widehat{\boldsymbol{\Phi}}$ is optimized by EWOA. The fitness function can be expressed as

$$Fitness = \sum_{i}^{N} \frac{1}{2}(\overline{\tau}_i - \hat{\boldsymbol{\tau}}_i)^{\mathrm{T}}(\overline{\tau}_i - \hat{\boldsymbol{\tau}}_i), \tag{22}$$

where N is the samples number, $\overline{\tau}_i$ represents the measured torque of the i test data, and $\widehat{\boldsymbol{\tau}}_i$ represents the calculation torque from Eq. (21).

The identification parameters $\widehat{\boldsymbol{\Phi}}$ of exoskeleton is obtained based on the EWOA as the fitness function is the smallest value, as shown in Table 4.

4 Experiments and Results

In this section, the excitation trajectory in Section 3.2 is used to drive the exoskeleton experimental data. Based on the EWOA, the model parameters are identified by using the collected dataset. Then the backstepping controller was designed based on the exoskeleton model after parameter identification. The model accuracy is verified through human-robot cooperative motion experiments.

4.1 Experimental Description and Data Processing

The excitation trajectory is regarded as the desired demand trajectory. A PID controller is used to drive a two-DOF lower limb exoskeleton experimental platform. According to the data collected by the encoder and torque sensor, the regression matrix $\boldsymbol{Y}$ and $\boldsymbol{\Phi}$ are obtained after filtering. The model parameters are calculated from the regression matrix and the torques. The accuracy of the model parameters can be verified by comparing the calculated with actual torques. In addition, some other test trajectories different from the excitation trajectory are used to verify the identification accuracy. Finally, the control experiment of the lower limb exoskeleton is realized by the backstepping controller.

The Butterworth low-pass filter is used to address the driving torque noise. In order to prevent the phase change of the filtered torque, both forward and reverse filtering are adopted to filter the torque signal as shown in Figure 5. In Figure 6, the blue curve represents the measured joint torque, and the red curve represents the calculated torque by the identification model. The experimental results show that the actual driving torque has a high fitness to the calculated torque. However, some

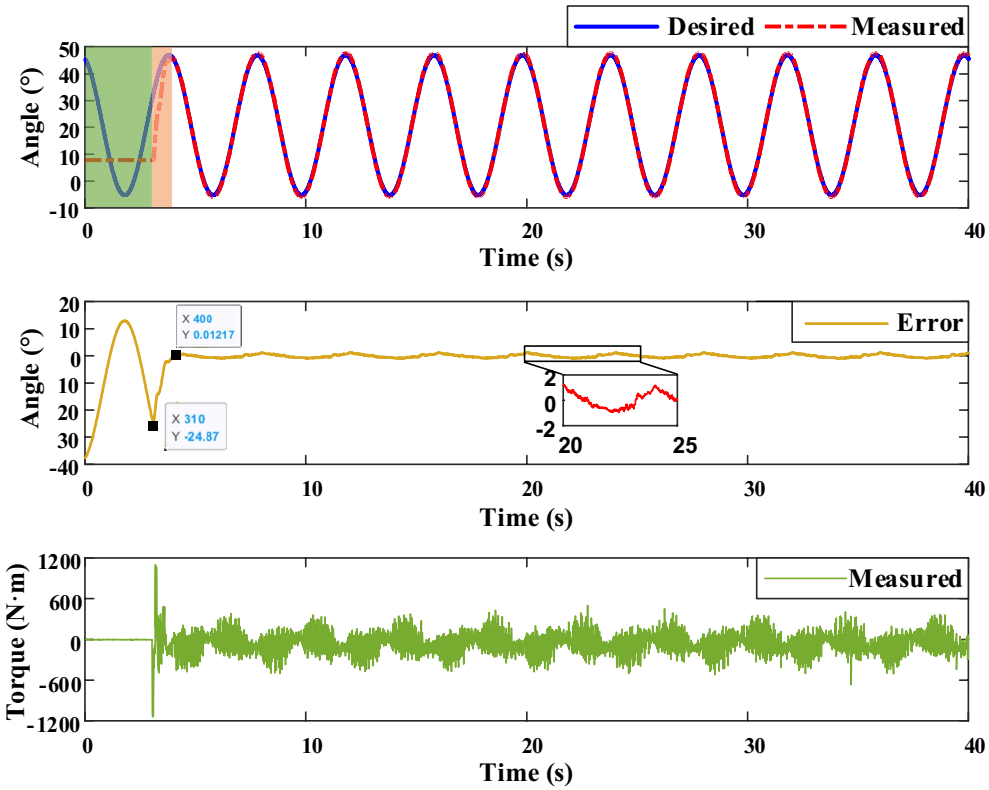

Figure 10 The joint position, and the corresponding position error, together with the measured torque of knee joint by using backstepping controller

discrete point errors are large due to unknown friction near the joint.

The measured and estimated torques for the steady state are compared in Figures 7 and 8. The results show that the estimated torque is consistent with the measured torque.

4.2 Model-Based Control

The model-based control is designed based on the exoskeleton parameters identification. In this study, a backstepping controller (7) [31] is used to improve both the wearable comfortable performance of operator and the real-time following error is constrained in a satisfactory boundary.

If the exoskeleton state variables are defined as $\boldsymbol{x}_1 = [\theta_1, \theta_2]^{\mathrm{T}}$, $\dot{\boldsymbol{x}}_1 = [\dot{\theta}_1, \dot{\theta}_2]^{\mathrm{T}}$, then the state space model of the exoskeleton dynamics yields that

$$\begin{cases} \dot{\boldsymbol{x}}_1 = \boldsymbol{x}_2, \\ \dot{\boldsymbol{x}}_2 = \boldsymbol{H}^{-1}(\tau - \boldsymbol{C}\boldsymbol{x}_2 - \boldsymbol{G} - \boldsymbol{f}). \end{cases} \tag{23}$$

The desired trajectory $\boldsymbol{x}_d = [\theta_{1d}, \theta_{2d}]^{\mathrm{T}}$, and the desired joint velocities $\dot{\boldsymbol{x}}_d = [\dot{\theta}_{1d}, \dot{\theta}_{2d}]^{\mathrm{T}}$ of the exoskeleton joint are selected as arbitrary trajectoris constrained in Table 2. The values of $\boldsymbol{H}$, $\boldsymbol{C}$, $\boldsymbol{G}$ are determined by the identified parameters $\widehat{\boldsymbol{\Phi}}$ in Eq. (12).

The state errors of exoskeleton $\delta_1 \in \mathbb{R}^2$, $\delta_2 \in \mathbb{R}^2$ are defined as

$$\begin{cases} \delta_1 = x_1 - x_d, \\ \delta_2 = x_2 - \alpha, \end{cases} \tag{24}$$

where $\alpha = -K_1\delta_1 + \dot{x}_d$ is the virtual control quantity, and $\boldsymbol{K}_1 = \mathbb{R}^{2\times 2}$ is a positive definite matrix.

Hence, the controller is designed as

$$\boldsymbol{\tau} = -\boldsymbol{\delta}_1 - \boldsymbol{K}_2\boldsymbol{\delta}_2 + \boldsymbol{G} + \boldsymbol{C}\alpha + \boldsymbol{f} + \boldsymbol{H}\dot{\alpha}, \tag{25}$$

where $\boldsymbol{K}_2 = \mathbb{R}^{2\times 2}$ is a positive definite matrix.

Then the controller stability is analyzed by Lyapunov technique. Firstly, the Lyapunov function V_1 is designed as

$$V_1 = \frac{1}{2}\delta_1^{\mathrm{T}}\delta_2. \tag{26}$$

The derivative of V_1 yields that

$$\dot{V}_1 = \delta_1^{\mathrm{T}}(\delta_2 + \alpha - \dot{x}_d). \tag{27}$$

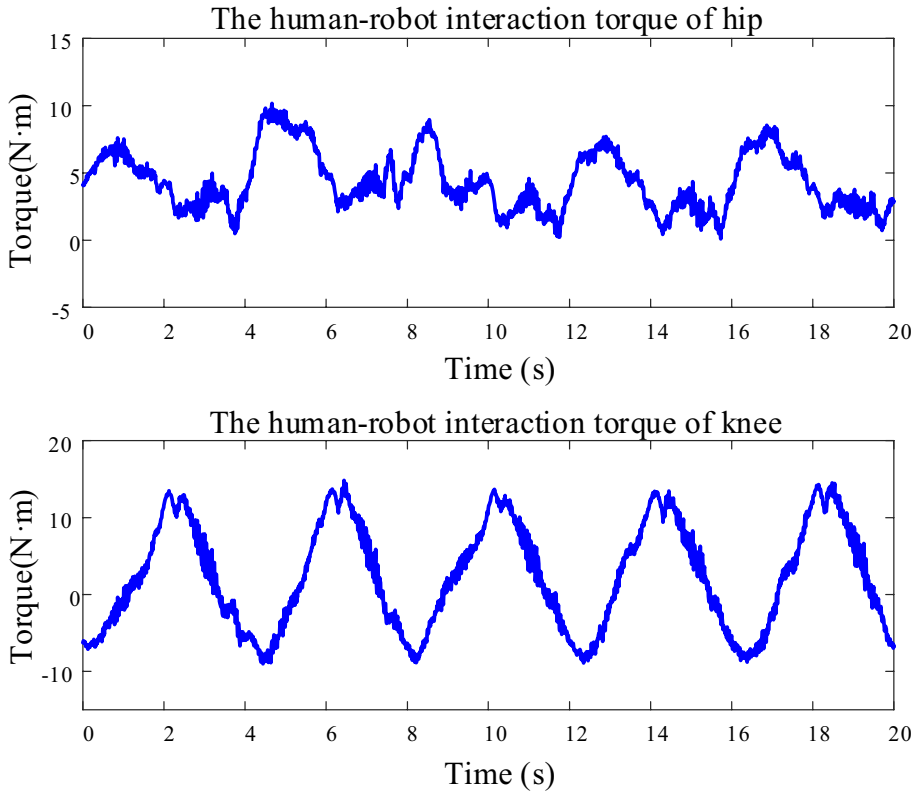

Figure 11 The steady state human-robot interaction torque by using backstepping controller

Meanwhile, the Lyapunov function V_2 is designed as

$$V_2 = V_1 + \frac{1}{2}\delta_2^2 H \delta_2. \tag{28}$$

Similarly, the derivative of V_2 is given by

$$\dot{V}_2 = \dot{V}_1 + \delta_2^{\mathrm{T}} H \dot{\delta}_2 + \frac{1}{2}\delta_2^{\mathrm{T}} \dot{H} \delta_2. \tag{29}$$

Since $\dot{\boldsymbol{H}} - 2\boldsymbol{C}$ is an anti-symmetric matrix, then $1/2\delta_2^{\mathrm{T}}(\dot{\boldsymbol{H}} - 2\boldsymbol{C}) = 0$. Substituting the backstepping controller Eq. (25) into Eq. (29), we have

$$\dot{V}_2 = -\delta_1^{\mathrm{T}} K_1 \delta_1 - \delta_2^{\mathrm{T}} K_2 \delta_2, \tag{30}$$

which indicate the exoskeleton system is asymptotically convergence to 0, as $t \to 0$.

Finally, a demand trajectory of exoskeleton is selected as $x_d = \sin(0.5\pi t)$. The related experimental results are shown in Figures 9 and 10.

The controller starts at 3 s, and the position response is shown in Figures 9 and 10. The knee joint motion achieves a steady-state response after 0.5 s. Meanwhile, the position error of hip joint response is less than 0.03 rad after 0.9 s. Since the exoskeleton system changes from static to dynamic, the joint torque is enlarged in the transient response range but has a safe range value. As the system approaches a steady-state response, the joint torque is in the normal range and periodically changes along with the demand trajectory. The experimental results show that the exoskeleton control based on the mathematical model after parameter identification can achieve high precision. In addition, the steady state human-robot interaction torque of the two joints is constrained within 15 N · m as shown in Figure 11. This torque is within a reasonable range, which improves the human-robot wearable comfortable performance under cooperative motion.

5 Conclusions

In this study, the 2-DOF lower limb exoskeleton platform is constructed by the Lagrange model to verify the model parameters identification and backstepping control experiment. The enhanced whale optimization algorithm (EWOA) is presented to design the excitation trajectories and identify the unknown model parameters such as the mass, moment of inertia and mechanical size. The periodic excitation trajectories should consider the mechanical physical constraint in order to input the desired position demand of exoskeletons. Then a backstepping

controller based on the identified model is designed to improve the human-robot wearable comfortable performance under cooperative motion. The dynamic and steady state response of the exoskeleton is guaranteed to synchronize the operator's gait trajectories with satisfactory performance.

Acknowledgements
Not applicable.

Authors' Contributions
YS was in charge of the whole trial; JK proposed the method and wrote the manuscript; ZC and YW assisted with sampling and laboratory analyses; QG provided the laboratory resources and contributed to manuscript revisions. All authors read and approved the final manuscript.

Funding
Supported by National Key Research and Development Program of China (Grant No. 2022YFF0708903), Ningbo Municipal Key Technology Research and Development Program of China (Grant No. 2022Z006), and Youth Fund of National Natural Science Foundation of China (Grant No. 52205043)

Data availability
The data that support the findings of this study are available on request from the corresponding author, [Jiange Kou], upon reasonable request.

Declarations

Competing Interests
The authors declare no competing financial interests.

Received: 23 December 2022 Revised: 29 November 2023 Accepted: 23 February 2024
Published online: 18 March 2024

References

[1] K Anam, A Al-Jumaily. Active exoskeleton control systems: State of the art. *Procedia Engineering*, 2012, 41: 988-994.
[2] S Rupal, S Rafique, A Singla, et al. Lower-limb exoskeletons: Research trends and regulatory guidelines in medical and non-medical applications. *International Journal of Advanced Robotic Systems*, 2017, 14(6): 1729881417743554.
[3] Q Guo, Q Wang, X Li. Finite-time convergent control of electrohydraulic velocity servo system under uncertain parameter and external load. *IEEE Transactions on Industrial Electronics*, 2018, 66(6): 4513-4523.
[4] Z Chen, Q Guo, H Xiong, et al. Control and implementation of 2-DOF lower limb exoskeleton experiment platform. *Chinese Journal of Mechanical Engineering*, 2021, 34(1): 1-17.
[5] K Ayusawa, E Yoshida. Motion retargeting for humanoid robots based on simultaneous morphing parameter identification and motion optimization. *IEEE Transactions on Robotics*, 2017, 33(6): 1343-1357.
[6] M Li, X Liu. Maximum likelihood least squares based iterative estimation for a class of bilinear systems using the data filtering technique. *International Journal of Control, Automation and Systems*, 2020, 18(6): 1581-1592.
[7] E Wu, M Zhou, D Hu, et al. Self-paced dynamic infinite mixture model for fatigue evaluation of pilots' brains. *IEEE Transactions on Cybernetics*, 2020, 52(7): 5623-5638.
[8] S Zhang, S Wang, F Jing, et al. A sensorless hand guiding scheme based on model identification and control for industrial robot. *IEEE Transactions on Industrial Informatics*, 2019, 15(9): 5204-5213.
[9] X Yang, Y Ni. Least-squares estimation for uncertain moving average model. *Communications in Statistics-Theory and Methods*, 2021, 50(17): 4134-4143.
[10] M Gautier, P Poignet. Extended Kalman filtering and weighted least squares dynamic identification of robot. *Control Engineering Practice*, 2001, 9(12): 1361-1372.
[11] M Hossain, T Zhang, O Ardakanian. Identifying grey-box thermal models with Bayesian neural networks. *Energy and Buildings*, 2021, 238: 110836.
[12] W Kim, M Park, L Park. Probabilistic modeling and Bayesian filtering for improved state estimation for soft robots. *IEEE Transactions on Robotics*, 2021, 37(5): 1728-1741.
[13] Z Wei, C Zou, F Leng, et al. Online model identification and state-of-charge estimate for lithium-ion battery with a recursive total least squares-based observer. *IEEE Transactions on Industrial Electronics*, 2017, 65(2): 1336-1346.
[14] K Shah, M Adhyaru. Parameter identification of PWARX models using fuzzy distance weighted least squares method. *Applied Soft Computing*, 2014, 25: 174-183.
[15] E Madsen, O S Rosenlund, D Brandt, et al. Model-based on-line estimation of time-varying nonlinear joint stiffness on an e-series universal robots manipulator. *2019 International Conference on Robotics and Automation (ICRA)*, *IEEE*, 2019: 8408–8414.
[16] M Gautier, A Janot, P O Vandanjon. A new closed-loop output error method for parameter identification of robot dynamics. *IEEE Transactions on Control Systems Technology*, 2012, 21(2): 428-444.
[17] J Kim. Collision detection and reaction for a collaborative robot with sensorless admittance control. *Mechatronics*, 2022, 84: 102811.
[18] S Lu, X Wang. A new methodology to estimate the rotating phase of a BLDC motor with its application in variable-speed bearing fault diagnosis. *IEEE Transactions on Power Electronics*, 2017, 33(4): 3399-3410.
[19] J Swevers, C Ganseman, B Tukel, et al. Optimal robot excitation and identification. *IEEE Transactions on Robotics and Automation*, 1997, 13(5): 730-740.
[20] T Katsumata, B Navarro, V Bonnet, et al. Optimal exciting motion for fast robot identification. Application to contact painting tasks with estimated external forces. *Robotics and Autonomous Systems*, 2019, 113: 149-159.
[21] Y Han, J Wu, C Liu, et al. An iterative approach for accurate dynamic model identification of industrial robots. *IEEE Transactions on Robotics*, 2020, 36(5): 1577-1594.
[22] D Lee, G Bae, S Jung. A decentralized model identification scheme by random-walk RLS process for robot manipulators: Experimental studies. *International Journal of Control, Automation and Systems*, 2019, 17: 1856-1865.
[23] G Gao, G Sun, J Na, et al. Structural parameter identification for 6 DOF industrial robots. *Mechanical Systems and Signal Processing*, 2018, 113: 145-155.
[24] J Ghan, R Steger, H Kazerooni. Control and system identification for the Berkeley lower extremity exoskeleton (BLEEX). *Advanced Robotics*, 2006, 20(9): 989-1014.
[25] B Brahmi, M Driscoll, K Bojairami, et al. Novel adaptive impedance control for exoskeleton robot for rehabilitation using a nonlinear time-delay disturbance observer. *ISA transactions*, 2021, 108: 381-392.
[26] D Yousri, B Thanikanti, D Allam, et al. Fractional chaotic ensemble particle swarm optimizer for identifying the single, double, and three diode photovoltaic models' parameters. *Energy*, 2020, 195: 116979.
[27] N Pourmousa, M Ebrahimi, M Malekzadeh, et al. Parameter estimation of photovoltaic cells using improved Lozi map based chaotic optimization Algorithm. *Solar Energy*, 2019, 180: 180-191.
[28] S Chakraborty, K Saha, R Chakraborty, et al. An enhanced whale optimization algorithm for large scale optimization problems. *Knowledge-Based Systems*, 2021, 233: 107543.
[29] S Zhang, S Wang, F Jing, et al. Parameter estimation survey for multi-joint robot dynamic calibration case study. *Science China Information Sciences*, 2019, 62: 1-15.
[30] A Tika, J Ulmen, N Bajcinca. Dynamic parameter estimation utilizing optimized trajectories. *2020 IEEE/RSJ International Conference on Intelligent Robots and Systems (IROS)*, IEEE, 2020: 7300–7307.
[31] K Khalil. Adaptive output feedback control of nonlinear systems represented by input-output models. *IEEE Transactions on Automatic Control*, 1996, 41(2): 177-188.

Yan Shi born in 1981, is a full professor at *School of Automation Science and Electrical Engineering, Beihang University, China*. His research interests include mechatronic engineering, intelligent medical devices and energy-saving technologies of pneumatic systems.

Jiange Kou born in 1993, is currently studying towards the Ph.D. degree at *School of Automation Science and Electrical Engineering, Beihang University, China*. His research interests include exoskeleton system, human-machine interaction, automatic control, and human movement intention recognition.

Zhenlei Chen born in 1992, is currently a postdoctoral fellow at *School of Aeronautics and Astronautics, University of Electronic Science and Technology of China*. His current research interests include machine learning, nonlinear control, and robotic exoskeleton.

Yixuan Wang born in 1989, is currently a lecturer at *Engineering Training Center, Beihang University, China*. His research interests include measurement and control systems, automatic control, and UAV fuel power systems.

Qing Guo born in 1981, is a full professor at *School of Aeronautics and Astronautics, University of Electronic Science and Technology of China*. His research interests include robust and adaptive control, electro-hydraulics.